# Scaffold-free Efficient Light Harvesting Nanoparticles Based on One-pot Self-Assembly of Donor-Acceptor Aggregation Induced Emission Luminogens

Chuanqi Li[∂,⊥], Jiaxiang Yan[∂,⊥], Bohan Yin[‡,†], Qin Zhang[∂], Yingying Huang[∂], Jiareng Chen[∂], Fengqi Wang[∂], James Chung Wai Cheung[∂], Mo Yang[∂,§,#,*], Siu Hong Dexter Wong[‡,†,*]

[‡]School of Medicine and Pharmacy, Ocean University of China, Qingdao 266003, China;

[†]Laboratory for Marine Drugs and Bioproducts, Qingdao Marine Science and Technology Center, Qingdao 266237, China

[∂]Department of Biomedical Engineering, The Hong Kong Polytechnic University, Kowloon, Hong Kong 999077, China;

[§]The Hong Kong Polytechnic University Shenzhen Research Institute, Shenzhen. 518000, P.R. China;

[#]Research Institute for Sports Science and Technology, The Hong Kong Polytechnic University, Kowloon, Hong Kong 999077, China.

[⊥]Chuanqi Li and Jiaxiang Yan contributed equally to this work.

***Corresponding author:**

Mo Yang: mo.yang@polyu.edu.hk

Siu Hong Dexter Wong: dexterwong@ouc.edu.cn

ABSTRACT

Constructing highly efficient artificial light-harvesting (LH) systems via a scaffold-free approach for capturing and utilizing light energy to emulate photosynthesis-inspired energy transfer processes is a great challenge. Herein, we report an efficient light-harvesting nanoparticle (LHN) based on two derivatives of tetraphenylethylene as a donor/acceptor (D/A) pair in a skeleton compact and effective stacking prepared by simple ultrasound-assisted self-assembly within ~1 h in water for effective aggregation-induced emission (AIE) effect and intermolecular energy transfer. By simply adjusting the D/A mixture ratio, the LHN shows tunable multi-color emission (from cyan to near-infrared) with a remarkable energy transfer efficiency of 96.5% at a D/A ratio of 50:1 and attains a high antenna effect of 79.2 at a D/A ratio of 4000:1. Importantly, the LHN exhibits a nearly pure white light emission with color coordinates of (0.32, 0.35) at a D/A ratio of 300:1 with a high quantum yield of 51%. Moreover, our LHN shows high biocompatibility and brightness for cellular imaging in MCF-7 cells over 3 days. Compared to the direct excitation of acceptors in the uptaken LHN, it shows a ~14-fold enhancement for cell imaging brightness. This simple and effective fabrication strategy opens up possibilities for large-scale AIEgen-based light-harvesting systems as tunable multi-color luminescent materials and great potential applications in the fields of white light materials and real-time cellular imaging.

**Keywords:** Aggregation-induced emission, Light Harvesting, Efficient Energy Transfer, Luminescent Nanoparticles, Tunable Light Emission

## INTRODUCTION

In the field of artificial light harvesting systems (LHS) for organic photovoltaics and bioimaging agents, the efficient capture and transfer of light represent a critical challenge in current research.[1] Drawing inspiration from the natural photochemical processes underlying biological photosynthesis, engineered LHSs have been developed to achieve effective harvesting of light energy through the phenomenon of Förster resonance energy transfer (FRET) - the non-radiative transfer of excitation from light-absorbing donor to light-emitting acceptor molecular species.[2-6] Generally, the LHSs can be synthesized by strategically affixing donor/acceptor (D/A) chromophores to a variety of structural scaffolds, including vesicles,[7] micelles,[8, 9] nanoparticles, [10] nanocrystals,[11] hydrogels[12, 13] and biomolecules,[14, 15] whose ordered and compact organization of multichromophores can enhance the efficiency of energy transfer ($\Phi_{ET}$) and reduce self-quenching. These approaches can be broadly classified into two groups, a scaffold framework and self-assembly. The former ascertains stability and controlled system but often requires substantial construction efforts. The latter can be simply fabricated by hydrophobic D/A chromophores at optimized conditions but may tend to be unstable and cause aggregation-induced quenching (ACQ) effect.[16] Moreover, most of these LHSs were fabricated in organic solvents instead of the aqueous environment like in nature. Thus, designing and fabricating highly efficient light-harvesting systems especially by the method of self-assembly that can operate effectively in aqueous environments remains a great challenge.

Aggregation-induced emission luminogens (AIEgens) can conquer the issue of ACQ and permit efficient molecular stacking at a high concentration in an aggregated state.[17] This concentrated stacking of AIEgens can lead to the restriction of intramolecular motion (RIM) at the aggregated state that weakens vibronic coupling and greatly reduces the probability of nonradiative transitions

for ultrabright emission.[18] Several studies reported the possibility of building up a photonic antenna for luminescence using AIEgens but required complex procedures to construct a confined system to restrict the pre-defined D/A ratio in the nanoscale.[7, 19] Scaffold-based light-harvesting platforms, particularly those employing DNA origami techniques or protein-based frameworks, excel in providing precise control over the spatial arrangement of chromophores.[20-23] For example, Stein et al. created a two-dimensional DNA origami structure that functions as a molecular breadboard, enabling precise and programmable fluorophore arrangement.[23] This design facilitates multistep energy transfer in a photonic wire-like setup, with "jumper" dyes used to manipulate energy-transfer paths. Bischoff et al. engineered a protein-based system that mimics energy transfer between photosynthetic light-harvesting components, using asymmetric, site-selective protein-protein conjugation with noncanonical amino acids for efficient energy transfer.[22] The scaffold's capacity to precisely control inter-component spacing provides a crucial advantage in enhancing energy transfer efficiency. This exacting structural organization enables the fine-tuning of molecular distances, a critical factor in optimizing the flow of energy through the light-harvesting system. However, the complexity involved in their fabrication often poses substantial challenges for large-scale production, potentially hindering widespread application.[24] Furthermore, their performance and structural integrity can be compromised when exposed to diverse environmental conditions, raising concerns about their long-term stability and adaptability in real-world scenarios. Potentially, a scaffold-free one-step self-assembly synthesis based on AIEgens is highly desirable to offer a cost-effective and simple approach for reproduction on a large scale for studying the mechanism and optimizing the performance of light-harvesting nanostructures.[25, 26]

Herein, we report AIEgen-driven light-harvesting nanoparticles (AIE-LHN) constructed by one-step ultrasound-assisted self-assembly for highly efficient energy transfer and tunable multicolor

luminescence with a wide photoluminescence spectrum (**Figure 1a**). We select 4-(1,2,2-triphenylvinyl)benzaldehyde (TPE-CHO) and 2-(3-cyano5,5-dimethyl-4-(4-(1,2,2-triphenylvinyl)styry-l)furan-2(5H)ylid-ne) malononitrile benzaldehyde (TPE-CHO-TCF) as an excellent donor/acceptor pair whose optical absorption/excitation and emission spectra largely overlap with each other to facilitate efficient FRET-based energy transfer. Moreover, the AIEgen pair shares a common TPE backbone for π-π stacking and potentially forms hydrogen bonds or dipole-dipole interactions between CHO and TCF groups,[27] together ascertaining tight molecular packing in the aqueous medium. In this study, we demonstrated that the AIE-LHN was generally synthesized by 3 min ultrasonication of the donor and acceptor molecules at various molar ratios, which were subsequently left undisturbed for self-assembly in aqueous medium within 1 h (**Figure 1a**). Our findings showed that the luminescent color of our AIE-LHN was tunable via regulating the D/A ratios from 4000:1 to 50:1, resulting in the color shifting from cyan to red/near-infrared (NIR) range and also white color (300:1). Remarkably, an ultrahigh $\Phi_{ET}$ at 96.5% was achieved at the D/A ratio of 50:1 and a high antenna effect (AE) at 79.2 at the D/A ratio of 4000:1. Moreover, this AIE-LHN exhibited good biocompatibility with a large Stokes shift > 230 nm, fast cellular entry and stable bioimaging signals over 72 h. The light-harvesting nanoparticle obtained by this cost-effective approach exhibits comparable optical performance to other existing light-harvesting systems constructed by complex scaffold-based strategies (**Table S1**). Such a simple strategy provides a one-step synthesis of AIEgen-based LHN for excellent light harvesting and tunable on-demand emission that potentially offers large-scale production for broad application prospects in biological imaging, fluorescent ink, and photovoltaic systems.

## EXPERIMTENTAL SECTION

**Chemicals and reagents.** Unless otherwise noted, all reagents were obtained from commercial suppliers and used without further purification. The solvents used in spectrum analysis are all HPLC grade. Deionized (DI) water (Millipore) was used in all aqueous experiments.

**Preparation of AIEgen-based light-harvesting nanoparticle (AIE-LHN).** 4-(1,2,2-triphenylvinyl)benzaldehyde (TPE-CHO, donor, 95%) and tetraphenylethylene (TPE, 97%) were purchased from Alfa Chemical, China. 2-(3-cyano5,5-dimethyl-4-(4-(1,2,2-triphenylvinyl)styry-l)furan-2(5H)ylid-ne) malononitrile benzaldehyde (TPE-CHO-TCF, acceptor) was synthesized through the reaction between TPE-CHO (0.001 mol) and compound 1 (0.003 mol) (Figure S1) with the presence of 1 mM NaOH (J&K Scientific, Hong Kong) in 5 mL ethanol under condense reflux. The final product was purified by high-performance liquid chromatography (HPLC, Thermo Scientific™ Dionex™) and was characterized by $^{1}$H nuclear magnetic resonance (NMR, Bruker Advance-III 600 MHz FT-NMR System). Next, the donor (D, 100 μg) and the acceptor (A, 100 μg) were dissolved in 100 μL dimethyl sulfoxide (DMSO), respectively. Then, an aliquot of D and A (50 μL in total) was simultaneously injected into 1 mL DI water at various D/A molar ratios (from 4000:1 to 50:1) under the ultrasonic condition (Branson 2800 CPXH ultrasonic cleaner, 40 Hz, 120 W). After 3 min of ultrasonication, the sample was left undisturbed within 1 h to obtain AIE-LHN. The same method was used to prepare TPE/TPE-CHO-TCF LHN (AIE-LHN) at various molar ratios.

**Material and optical property characterizations.** The hydrodynamic diameter and zeta potential of the samples were measured by Zetasizer Nanosystem (Malvern Instruments). Nanoparticles were diluted with DI water in 10 mg/mL for the measurement. The Fluorescence spectra were measured by a fluorescence spectrometer (Shimadzu RF-5301 PC). The fluorescence images were recorded under confocal laser scanning microscopy (CLSM, Leica TCP SP5).

Transmission electron microscopy and high-resolution transmission electron microscopy (HR-TEM) images of the nanoparticles were taken by Tecnai G2 F20 S-TWIN microscope, operating at 120 kV. The TEM specimens were prepared by gently placing a carbon-coated copper grid on the surface of the sample. After that, the TEM grid was removed, stained with an aqueous solution of 2% phosphotungstic acid, dried for 0.5 h at room temperature, and then subjected to TEM observation. Fluorescence absolute quantum yields were collected on a fluorescence spectrometer with a calibrated integrating sphere system (Horiba Jobin Yvon-Edison Fluoromax-4). To reduce the fluctuation of the excitation intensity, the lamp was switched on 1 h prior to the experiment. The CIE-1931 chromaticity coordinates were calculated using a Color Coordinate.exe program. Time-resolved fluorescence spectroscopy (TRES) was measured on a Fluorolog-3 spectrofluorometer (Horiba JobinYvon) with a Delta Diode (370 nm, DD-375, Horiba Scientific) as the excitation source and a picosecond photon detection module (PPD-850, Horiba Scientific) as the detector. During the measurements, the data points were collected at 10 nm intervals with a wavelength range of 440-680 nm.

**Calculations of energy-transfer efficiency ($\Phi_{ET}$).**[28] Energy-transfer efficiency, $\Phi_{ET}$, the fraction of the absorbed energy that is transferred to the acceptor was experimentally measured as a ratio of the fluorescence intensities of the donor in the absence and presence of the acceptor:

$$\Phi_{ET} = 1 - I_{DA} / I_D \quad \text{.....(1)}$$

where $I_{DA}$ and $I_D$ are the intensity of the donor's (TPE-CHO) fluorescence emission with and without the acceptor (TPE-TCF), respectively. The excitation wavelength is 372 nm.

**Average number of donor molecules quenched by single acceptor ($K_{SV}$).**[29] The number of the donor molecules quenched by a single acceptor molecule was determined using the Stern-Volmer equation:

$$F_0 / F = 1 + K_{SV}[A] \quad \text{.....(2)}$$

where $F_0$ and $F$ are TPE-CHO fluorescence intensities (λ= 480 nm) in the absence and presence of the acceptor, respectively, $K_{SV}$ is the Stern-Volmer quenching constant, and [A] is the concentration of the acceptor. The quenching constant is obtained from the slope of a linear fit to a plot of $F_0/F$ versus [A]. If the acceptor concentration is expressed as a molecule fraction (A:D), $K_{SV}$ represents the number of donor molecules quenched by a single acceptor.

**Antenna effect.**[7] A high antenna effect (AE) can significantly improve the light-harvesting efficiency.[30] To evaluate the light-harvesting efficiency of our AIE-LHN, we quantified it using the antenna effect. This effect is measured as the ratio of the fluorescence of the acceptor when the donors are excited to the fluorescence of the acceptor upon its direct excitation at given excitation wavelengths.[20] The parameter of the antenna effect was estimated according to the following equation:

$$\mathrm{AE} = \frac{I^{610nm}_{D+A(\lambda ex=372nm)} - I^{610nm}_{D(\lambda ex=372nm)} \times f}{I^{610nm}_{D+A(\lambda ex=475nm)}} \quad \text{.....(3)}$$

where $I_{D+A}$ ($\lambda_{ex}$ = 372 nm) is the emission intensity of TPE-CHO-TCF ($\lambda_{ex}$ = 372 nm) in AIE-LHN, $I_{D+A}$ ($\lambda_{ex}$ = 475 nm) is the emission intensity of TPE-CHO-TCF ($\lambda_{ex}$ = 475 nm) in AIE-LHN ($\lambda_{ex}$ = 372 nm), $I_D$ is the emission intensity of TPE-CHO ($\lambda_{ex}$ = 372 nm) in TPE-CHO NPs**,** and $f$ is the correction factor, which is calculated via the ratio of the emission intensity of TPE-CHO ($\lambda_{ex}$ = 372 nm) in AIE-LHN to that of TPE-CHO ($\lambda_{ex}$ = 372 nm) in TPE-CHO only NPs.

**Cytotoxicity analysis.**[31] To evaluate the cytotoxicity of our AIE-LHN, we utilized the Cell Counting Kit-8 (CCK-8) assay from Beyotime, China, using MCF-7 breast cancer cells as our model system. The experimental procedure involved seeding MCF-7 cells in 96-well plates at a density of $1.5 \times 10^4$ cells per well and allowing overnight attachment. These cells were then

exposed to AIE-LHN at concentrations ranging from 0 to 100 μg/mL for either 12 or 24 hours. Following treatment, CCK-8 reagent was added to each well and incubated for 3 hours. Cell viability was subsequently quantified by measuring absorbance at 450 nm using an automated microplate reader, enabling us to assess the dose-dependent and time-dependent effects of AIE-LHN on cell viability. The cell viability was calculated by:

$$\text{Cell viability (\%)} = \frac{A_{sample} - A_{blank}}{A_0 - A_{blank}} \times 100 \quad \text{.....(4)}$$

In this equation, $A_{sample}$ represents the absorbance measured in wells containing cells treated with AIE-LHN, $A_{blank}$ denotes the absorbance of wells without any cells (serving as a background control), and $A_0$ indicates the absorbance of wells with untreated cells (representing 100% viability).

**Intracellular imaging.** The experimental procedure involved seeding MCF-7 cells in a confocal dish at a density of $1.0\times10^5$ cells, allowing them to attach overnight. The cells were then incubated with AIE-LHN at a concentration of 50 μg/mL for 12 hours. Before observation, excess AIE-LHN was removed, and the cells were washed with cold PBS. The AIE-LHN was excited at 372 nm to collect TPE-CHO and TPE-CHO-TCF channels, and at 488 nm for direct excitation of TPE-CHO-TCF. Fluorescent images were captured at 430-490 nm and 600-700 nm using confocal laser scanning microscopy.

## RESULTS AND DISCUSSION

The emission spectrum of TPE-CHO ($\lambda_{ex}/\lambda_{em}$ = 375 nm/485 nm) showed a large overlapping area with the absorption spectrum of TPE-CHO-TCF ($\lambda_{ex}/\lambda_{em}$ = 480 nm/610 nm), thereby making them a good D/A pair (**Figure 2a**). We constructed donor-only TPE-CHO nanoparticles (NPs) as control or AIE-LHN of various D/A molar ratios (4000:1 to 50:1) by adding a trace amount of dimethyl sulfoxide (DMSO)-dissolved molecules into water under ultrasonication for 3 min,

followed by undisturbed for self-assembly within 1 h (**Figure 1a and Figure S1-3**). The molecules co-aggregated with each other through hydrophobic interactions and intermolecular interactions,[32] forming spherical NPs (**Figure 1b**). TPE-CHO NPs alone or the addition of acceptor molecules to TPE-CHO produced NP sizes of ~50 nm, at the equivalent total amount (**Figure 1b and Table S2**). All NPs showed a negative zeta potential of ~20 mV for all groups (**Table S2**), indicating a strong electrostatic repulsion force to ascertain colloidal stability in water. Consistently, the excited NP solution showed the Tyndall effect, suggesting the presence of colloids in nano size (**Figure 1b, inset**).

Next, we assessed the optical properties of the AIE-LHN with various D/A ratios. We showed that AIE-LHN with decreased D/A ratios showed a trend of reduced peak emission intensity at 485 nm (donor) and increased 610 nm peak emission (**Figure 2b**), consistent with the results of the FRET effect.[33] We further studied the energy transfer process in AIE-LHN by its fluorescence lifetime decay. The lifetime of the donor emission at 485 nm was 2.14 ns without acceptor and decreased continuously with increasing amounts of acceptor doped into the mixture, to 0.45 ns at a 100:1 donor/acceptor ratio (**Figure 2c**). The lifetime of the acceptor only was 0.39 ns (**Figure S7**), shorter than the donor's and even less than that in a 100:1 donor/acceptor ratio, indicating efficient energy transfer from donor to acceptor. At 100:1 D/A ratio, the time-resolved fluorescence spectra excited at 372 nm displayed a decrease of donor emission ($\lambda_{em}$ = 485 nm) within 2 ns, accompanied by a sharp increase of the acceptor emission ($\lambda_{em}$ = 610 nm) (**Figure 2d**). Moreover, the RGB emission of AIE-LHN can be arbitrarily adjusted by simply changing the D/A ratio. With the increased D/A ratio, the RGB color of the AIE-LHN gradually shifted from cyan to orange-red (**Figure 2e**). It is worth noting that a sample with a D/A ratio of 300:1 exhibits nearly pure white light emission with color coordinates of (0.32, 0.35), very close to the exact white point

(0.33, 0.33). White light organic materials have high potential in display and lighting.[34] Moreover, the quantum yield ($\Phi_F$) of AIE-LHN at this white light ratio was 51% (57% for TPE-CHO NPs), which is the highest value reported so far for white light-emitting organic materials in water. In addition, we demonstrated this diverse RGB color emission by injecting the AIE-LHN solution with D/A ratios at 4000:1, 300:1, and 50:1, respectively, into microfluidic channels to visualize color-emission tuning possibilities within the imprinted letter "U" (**Figure 2f**).

Furthermore, we assessed that $\Phi_{ET}$ of AIE-LHN increased with decreased D/A ratios that strikingly reached 92.2% and 96.5% at D/A ratios of 100:1 and 50:1, respectively (**Figure 3a**). Even at the high D/A ratio of 4000:1, the AIE-LHN still possessed a significant $\Phi_{ET}$ (10.4%), highlighting the efficiency of the system. Meanwhile, the antenna effect (AE, a factor about how much brighter the acceptor emits when excited by the donor) of the AIE-LHN showed a reversed trend of that of $\Phi_{ET}$ corresponding to the D/A ratios (**Figure 3b**). In particular, an ultrahigh AE close to 80 and a Ksv value (the average number of donor molecules quenched by a single acceptor calculated by linear curve-fitting of the Stern-Volmer plot of the donor as a function of the donor/acceptor ratio) of 781 were obtained at the D/A ratio of 4000:1 (**Figure 3b-c**). Also, the fluorescent intensity of the acceptor acquired energy from the donor was ~120 times the acceptor excited directly by the laser at 475 nm in D/A ratio of 100:1, for instance (**Figure 3d and Figure S4**), highlighting the importance of efficient energy transfer to the acceptor from multiple excited donors in close proximity. Overall, these performances outperform or are comparable to the majority of recently reported artificial light-harvesting systems fabricated by complex scaffold-based strategies. (**Table S1**).

We hypothesize that the molecular structure of the AIEgen-based donor/acceptor pair is also a critical factor influencing energy transfer efficiency apart from the absorption/emission

overlapping. To explore this effect, we synthesized the LHN that paired TPE ($\lambda_{ex}/\lambda_{em}$ = 372 nm/475 nm, the same absorption/emission spectra as that of TPE-CHO) and TPE-CHO-TCF molecules to form TPE/TPE-CHO-TCF based LHN (TPE-LHN) of various D/A ratios (**Figure 3e**). Strikingly, the fluorescent intensity of the acceptor was minimally increased with decreased D/A ratios. For example, the emission peak intensity at 610 nm of TPE-LHN was 100-fold less than those in AIE-LHN at the D/A ratio of 100:1. Consistently, the $\Phi_F$ of TPE-CHO NPs and AIE-LHN were 58.7% and 40.3%, respectively, while the $\Phi_F$ of TPE NPs and TPE-LHN were 15.9% and 14.5%, respectively (**Figure 3f**). This large difference in $\Phi_F$ still existed between AIE-LHN and TPE-LHN after the addition of the acceptor to TPE NPs. Theoretically, both TPE and TPE-CHO possess a higher HOMO-LUMO energy gap compared to TPE-CHO-TCF for an efficient resonance energy transfer process between the donor and acceptor (**Figure 4**).[35, 36] Also, the LUMO and HOMO of both donors respectively show higher and lower energies than those in the acceptor for pronounced D/A structure. Note that both TPE-CHO and TPE-CHO-TCF possess polar side groups that potentially form intermolecular hydrogen bondings and dipole-dipole interaction in aggregated state in aqueous medium, while TPE only has symmetric phenyl groups on each side (**Figure S5**). Such interactions can strengthen intermolecular stacking which further reinforces the RIM phenomenon for enhanced AIE effect and energy transfer efficiency.[37, 38] On the other hand, the presence of the polar side groups of TPE-CHO-TCF can cause repulsion to the nonpolar TPE molecules from high to low D/A ratio within the LHN that weakens the intermolecular interactions and abrogates FRET efficiency.[39, 40] Therefore, we propose that TPE-CHO and TPE-CHO-TCF form a good D/A pair to build up our efficient light harvesting system.

Our constructed AIE-LHN at D/A ratio of 100:1 and 50:1 showed a Stokes shift of more than 230 nm from the excitation of the donor (peak absorption at 372 nm) to the emission of the acceptor

(peak emission at 610 nm) (**Figure 2b**) and exhibited broad emission spectra with the full width at half-maxima (FWHM) over 150 nm reaching the near-infrared (NIR) emission (650–900 nm) region (**Figure S6**). These properties make it an ideal luminescent nanomaterial for cell imaging to avoid autofluorescence interference and crosstalk between different channels in cells.[41-43] The fluorescence emission intensity at 610 nm reaches its maximum when the D/A ratio is 80:1. As the D/A ratio decreases from this optimal point, we observe a subtle decline in the emission intensity (**Figure S8)**. This trend suggests that the 80:1 ratio represents the most efficient composition for maximizing the fluorescence output at the specified wavelength. Considering the potential bioapplications of the AIE-LHN, we evaluated the cytotoxicity of the AIE-LHN over various concentrations for 24 and 48 h. Our results indicated nearly negligible cytotoxicity (>85% cell viability) up to a concentration of 100 μg/mL AIE-LHN in MCF-7 cells after the incubation (**Figure S9**). Moreover, the AIE-LHNs were efficiently internalized into the cells after 4 h of incubation (**Figure 5a-b**). As a control, TPE-CHO NPs uptaken by the cells did not show emission from that of the acceptor (**Figure 5a**). With the decreased D/A ratio, the emission intensity of the TPE-CHO-TCF increased (D/A ratio from 300:1 to 50:1), consistent with the solution-based experiment (**Figure 2**). In contrast, direct excitation of the acceptor at the same condition resulted in weak emission (**Figure 5a**). In particular, the mean fluorescence intensity enhancement times of AIE-LHN at 100:1 and 50:1 compared to the directly excited acceptor in AIE-LHN were 11.4 and 14.2, respectively. Finally, we showed that the fluorescent signal of the uptaken AIE-LHN by cells remained highly stable over 72 h with an overall 30% dropped signal, indicating a potential application for ultrabright bioimaging and two weeks of cellular tracking using AIE-LHN. In addition, our 14-day stability analysis revealed that AIE-LHN maintained exceptional consistency in both hydrodynamic size and fluorescence intensity, indicating robust stability in solution over

an extended period (**Figure S10**). These findings highlight that our AIE-LHN can maintain its efficient energy transfer processes in complex physiological conditions and is suitable for cellular imaging.

## CONCLUSIONS

In conclusion, we report an AIEgen-driven highly efficient artificial light-harvesting nanoparticle synthesized via a simple ultrasound-assisted self-assembly method achieved within ~1 h. By simply tuning the mixture ratio of the donor (TPE-CHO) and acceptor (TPE-TCF) from 4000:1 to 50:1, we demonstrate a tunable multi-color RGB spectrum (from cyan to NIR range) and well-performing light-harvesting properties. Notably, the achieved $\Phi_{ET}$ of the AIE-LHN is 96% at D/A ratio of 50:1 and its high D/A of 4000:1 shows a remarkable AE of 79.2 with Ksv of 781, highlighting its exceptional light harvesting efficiency. Such a high efficiency is potentially attributed to the multiple intermolecular interactions such as π-π interactions and dipole-dipole/hydrogen bondings between TPE-CHO and TPE-CHO-TCF molecules in the NP to underpin AIE and FRET effect. Besides, this system shows good performance in fluorescent imaging of the living MCF-7 cells and stable fluorescent output over 72 h. Our AIEgen-driven design will open a new avenue for developing tunable multi-color luminescent materials based on such a simple and effective synthesis strategy and show great potential applications in the fields of optical materials, bio-imaging, and light-harvesting devices.

ASSOCIATED CONTENT

**Supporting Information**

The following files are available free of charge on the ACS Publications website. Comparison of different reported light-harvesting systems with this work, additional characterizations of AIE-LHN at various D/A ratios, synthetic route of TPE-CHO-TCF, and $^{1}$H-NMR spectrum of TPE-CHO.

AUTHOR INFORMATION

**Corresponding Author**

*E−mail (M. Yang): mo.yang@polyu.edu.hk

*E−mail (S. H. D. Wong): dexterwong@ouc.edu.cn

**Author Contributions**

$^{\perp}$These authors contributed equally: C. L. and J. Y.

**Notes**

The authors declare no competing financial interest.

ACKNOWLEDGMENTS

This work was supported by the Shenzhen Science and Technology Program-Basic Research Scheme (JCYJ20220531090808020), the Hong Kong Research Grants Council (RGC) Collaborative Research Fund (C5005-23W and C5078-21E), the Research Grants Council (RGC) Hong Kong General Research Fund (15217621 and 15216622), the Guangdong-Hong Kong Technology Cooperation Funding Scheme (GHP/032/20SZ and SGDX20201103095404018), the

Hong Kong Polytechnic University Internal Fund (1-YWB4, 1-WZ4E, 1-CD8M, 1-WZ4E, 1-CEB1, 1-YWDU, 1-CE2J and 1-W02C). We also would like to acknowledge the funding from Start-up Fundings of Ocean University of China (862401013154 and 862401013155), Laboratory for Marine Drugs and Bioproducts Qingdao Marine Science and Technology Center (no.: LMDBCXRC202401 and LMDBCXRC202402), Taishan Scholar Youth Expert Program of Shandong Province (tsqn202306102 and tsqn202312105), and Shandong Provincial Overseas Excellent Young Scholar Program (2024HWYQ-042 and 2024HWYQ-043) for supporting this work. This work was also supported by the University Research Facility in Life Sciences of the Hong Kong Polytechnic University.

REFERENCE


(1) Nelson, N.; Ben-Shem, A. The complex architecture of oxygenic photosynthesis. *Nat. Rev. Mol. Cell Biol.* **2004**, *5* (12), 971-982.

(2) Chen, X.-M.; Chen, X.; Hou, X.-F.; Zhang, S.; Chen, D.; Li, Q. Self-assembled supramolecular artificial light-harvesting nanosystems: construction, modulation, and applications. *Nanoscale Adv.* **2023**, *5* (7), 1830-1852.

(3) Mirkovic, T.; Ostroumov, E. E.; Anna, J. M.; Van Grondelle, R.; Govindjee; Scholes, G. D. Light absorption and energy transfer in the antenna complexes of photosynthetic organisms. *Chem. Rev.* **2017**, *117* (2), 249-293.

(4) Yim, D.; Sung, J.; Kim, S.; Oh, J.; Yoon, H.; Sung, Y. M.; Kim, D.; Jang, W.-D. Guest-induced modulation of the energy transfer process in porphyrin-based artificial light harvesting dendrimers. *J. Am. Chem. Soc.* **2017**, *139* (2), 993-1002.

(5) Jeong, Y. H.; Son, M.; Yoon, H.; Kim, P.; Lee, D. H.; Kim, D.; Jang, W. D. Guest‐induced photophysical property switching of artificial light‐harvesting dendrimers. *Angew. Chem. Int. Ed.* **2014**, *53* (27), 6925-6928.

(6) Lunz, M.; Bradley, A. L.; Gerard, V. A.; Byrne, S. J.; Gun'Ko, Y. K.; Lesnyak, V.; Gaponik, N. Concentration dependence of Förster resonant energy transfer between donor and acceptor nanocrystal quantum dot layers: Effect of donor-donor interactions. *Phys. Rev. B: Condens. Matter* **2011**, *83* (11), 115423.

(7) Li, C.; Zhang, J.; Zhang, S.; Zhao, Y. Efficient Light‐Harvesting Systems with Tunable Emission through Controlled Precipitation in Confined Nanospace. *Angew. Chem. Int. Ed.* **2019**, *58* (6), 1643-1647.

(8) Liu, Y.; Jin, J.; Deng, H.; Li, K.; Zheng, Y.; Yu, C.; Zhou, Y. Protein‐Framed Multi‐Porphyrin Micelles for a Hybrid Natural–Artificial Light‐Harvesting Nanosystem. *Angew. Chem. Int. Ed.* **2016**, *55* (28), 7952-7957.

(9) Hirayama, S.; Oohora, K.; Uchihashi, T.; Hayashi, T. Thermoresponsive micellar assembly constructed from a hexameric hemoprotein modified with poly (N-isopropylacrylamide) toward an artificial light-harvesting system. *J. Am. Chem. Soc.* **2020**, *142* (4), 1822-1831.

(10) Li, Y.; Dong, Y.; Cheng, L.; Qin, C.; Nian, H.; Zhang, H.; Yu, Y.; Cao, L. Aggregation-induced emission and light-harvesting function of tetraphenylethene-based tetracationic dicyclophane. *J. Am. Chem. Soc.* **2019**, *141* (21), 8412-8415.

(11) Chen, P. Z.; Weng, Y. X.; Niu, L. Y.; Chen, Y. Z.; Wu, L. Z.; Tung, C. H.; Yang, Q. Z. Light‐Harvesting Systems Based on Organic Nanocrystals To Mimic Chlorosomes. *Angew. Chem. Int. Ed.* **2016**, *55* (8), 2759-2763.

(12) Garain, S.; Garain, B. C.; Eswaramoorthy, M.; Pati, S. K.; George, S. J. Light‐harvesting supramolecular phosphors: highly efficient room temperature phosphorescence in solution and hydrogels. *Angew. Chem. Int. Ed.* **2021**, *60* (36), 19720-19724.

(13) Gorai, T.; Maitra, U. Luminescence resonance energy transfer in a multiple‐component, self‐assembled supramolecular hydrogel. *Angew. Chem. Int. Ed.* **2017**, *56* (36), 10730-10734.

(14) Garo, F.; Häner, R. A DNA‐based light‐harvesting antenna. *Angew. Chem.* **2012**, *4* (124), 940-943.

(15) Miller, R. A.; Presley, A. D.; Francis, M. B. Self-assembling light-harvesting systems from synthetically modified tobacco mosaic virus coat proteins. *J. Am. Chem. Soc.* **2007**, *129* (11), 3104-3109.
(16) Yan, S.; Gao, Z.; Yan, H.; Niu, F.; Zhang, Z. Combination of aggregation-induced emission and clusterization-triggered emission in mesoporous silica nanoparticles for the construction of an efficient artificial light-harvesting system. *J. Mater. Chem. B* **2020**, *8* (41), 14587-14594.
(17) Mei, J.; Leung, N. L.; Kwok, R. T.; Lam, J. W.; Tang, B. Z. Aggregation-induced emission: together we shine, united we soar! *Chem. Rev.* **2015**, *115* (21), 11718-11940.
(18) Hong, Y.; Lam, J. W.; Tang, B. Z. Aggregation-induced emission: phenomenon, mechanism and applications. *Chem. Commun.* **2009**, (29), 4332-4353.
(19) Tang, L.; Wu, Z.; Zhang, Q.; Hu, Q.; Dang, X.; Cui, F.; Tang, L.; Xiao, T. A sequential light-harvesting system with thermosensitive colorimetric emission in both aqueous solution and hydrogel. *Chem. Commun.* **2024**, *60* (35), 4719-4722.
(20) Hemmig, E. A.; Creatore, C.; Wünsch, B.; Hecker, L.; Mair, P.; Parker, M. A.; Emmott, S.; Tinnefeld, P.; Keyser, U. F.; Chin, A. W. Programming light-harvesting efficiency using DNA origami. *Nano Lett.* **2016**, *16* (4), 2369-2374.
(21) Li, Y.; Xia, C.; Tian, R.; Zhao, L.; Hou, J.; Wang, J.; Luo, Q.; Xu, J.; Wang, L.; Hou, C. "On/Off" Switchable Sequential Light-Harvesting Systems Based on Controllable Protein Nanosheets for Regulation of Photocatalysis. *ACS nano* **2022**, *16* (5), 8012-8021.
(22) Bischoff, A. J.; Hamerlynck, L. M.; Li, A. J.; Roberts, T. D.; Ginsberg, N. S.; Francis, M. B. Protein-Based Model for Energy Transfer between Photosynthetic Light-Harvesting Complexes Is Constructed Using a Direct Protein–Protein Conjugation Strategy. *J. Am. Chem. Soc.* **2023**, *145* (29), 15827-15837.
(23) Stein, I. H.; Steinhauer, C.; Tinnefeld, P. Single-molecule four-color FRET visualizes energy-transfer paths on DNA origami. *J. Am. Chem. Soc.* **2011**, *133* (12), 4193-4195.
(24) Zhou, X.; Satyabola, D.; Liu, H.; Jiang, S.; Qi, X.; Yu, L.; Lin, S.; Liu, Y.; Woodbury, N. W.; Yan, H. Two‐Dimensional Excitonic Networks Directed by DNA Templates as an Efficient Model Light‐Harvesting and Energy Transfer System. *Angew. Chem.* **2022**, *134* (51), e202211200.
(25) Xiao, T.; Zhang, L.; Chen, D.; Zhang, Q.; Wang, Q.; Li, Z.-Y.; Sun, X.-Q. A pillar [5] arene-based artificial light-harvesting system with red emission for high-resolution imaging of latent fingerprints. *Org. Chem. Front.* **2023**, *10* (13), 3245-3251.
(26) Xiao, T.; Ren, D.; Tang, L.; Wu, Z.; Wang, Q.; Li, Z.-Y.; Sun, X.-Q. A temperature-responsive artificial light-harvesting system in water with tunable white-light emission. *J. Mater. Chem. A* **2023**, *11* (34), 18419-18425.
(27) Jo, J.; Olasz, A.; Chen, C.-H.; Lee, D. Interdigitated hydrogen bonds: electrophile activation for covalent capture and fluorescence turn-on detection of cyanide. *J. Am. Chem. Soc.* **2013**, *135* (9), 3620-3632.
(28) Song, Q.; Goia, S.; Yang, J.; Hall, S. C.; Staniforth, M.; Stavros, V. G.; Perrier, S. b. Efficient artificial light-harvesting system based on supramolecular peptide nanotubes in water. *J. Am. Chem. Soc.* **2020**, *143* (1), 382-389.
(29) Zhang, W.; Luo, Y.; Ni, X.-L.; Tao, Z.; Xiao, X. Two-step, sequential, efficient, artificial light-harvesting systems based on twisted cucurbit [14] uril for manufacturing white light emission materials. *Chem. Eng. J.* **2022**, *446*, 136954.
(30) Li, J. J.; Chen, Y.; Yu, J.; Cheng, N.; Liu, Y. A Supramolecular Artificial Light‐Harvesting System with an Ultrahigh Antenna Effect. *Adv. Mater.* **2017**, *29* (30), 1701905.

(31) Bao, W.; Liu, M.; Meng, J.; Liu, S.; Wang, S.; Jia, R.; Wang, Y.; Ma, G.; Wei, W.; Tian, Z. MOFs-based nanoagent enables dual mitochondrial damage in synergistic antitumor therapy via oxidative stress and calcium overload. *Nat. Commun.* **2021**, *12* (1), 6399.
(32) Wang, H.; Zhao, E.; Lam, J. W.; Tang, B. Z. AIE luminogens: emission brightened by aggregation. *Mater. Today* **2015**, *18* (7), 365-377.
(33) He, X.; Xiong, L.-H.; Huang, Y.; Zhao, Z.; Wang, Z.; Lam, J. W. Y.; Kwok, R. T. K.; Tang, B. Z. AIE-based energy transfer systems for biosensing, imaging, and therapeutics. *TrAC, Trends Anal. Chem.* **2020**, *122*, 115743.
(34) Zhang, M.; Yin, S.; Zhang, J.; Zhou, Z.; Saha, M. L.; Lu, C.; Stang, P. J. Metallacycle-cored supramolecular assemblies with tunable fluorescence including white-light emission. *Proc. Natl. Acad. Sci.* **2017**, *114* (12), 3044-3049.
(35) Feron, K.; Belcher, W. J.; Fell, C. J.; Dastoor, P. C. Organic solar cells: understanding the role of Förster resonance energy transfer. *Int. J. Mol. Sci.* **2012**, *13* (12), 17019-17047.
(36) Wang, Y. J.; Shi, Y.; Wang, Z.; Zhu, Z.; Zhao, X.; Nie, H.; Qian, J.; Qin, A.; Sun, J. Z.; Tang, B. Z. A Red to Near‐IR Fluorogen: Aggregation‐Induced Emission, Large Stokes Shift, High Solid Efficiency and Application in Cell‐Imaging. *Chem. - A Eur. J.* **2016**, *22* (28), 9784-9791.
(37) Meher, N.; Panda, S.; Kumar, S.; Iyer, P. K. Aldehyde group driven aggregation-induced enhanced emission in naphthalimides and its application for ultradetection of hydrazine on multiple platforms. *Chem. Sci.* **2018**, *9* (16), 3978-3985.
(38) Peng, Q.; Shuai, Z. Molecular mechanism of aggregation‐induced emission. *Aggregate* **2021**, *2* (5), e91.
(39) Li, X.; Kohli, P. Investigating molecular interactions in biosensors based on fluorescence resonance energy transfer. *J. Phys. Chem. C* **2010**, *114* (14), 6255-6264.
(40) Yang, Y.; Huang, J.; Yang, X.; Quan, K.; Wang, H.; Ying, L.; Xie, N.; Ou, M.; Wang, K. FRET nanoflares for intracellular mRNA detection: avoiding false positive signals and minimizing effects of system fluctuations. *J. Am. Chem. Soc.* **2015**, *137* (26), 8340-8343.
(41) Li, Y.; Cai, Z.; Liu, S.; Zhang, H.; Wong, S. T.; Lam, J. W.; Kwok, R. T.; Qian, J.; Tang, B. Z. Design of AIEgens for near-infrared IIb imaging through structural modulation at molecular and morphological levels. *Nat. Commun.* **2020**, *11* (1), 1255.
(42) Zhang, Q.; Yin, B.; Hao, J.; Ma, L.; Huang, Y.; Shao, X.; Li, C.; Chu, Z.; Yi, C.; Wong, S. H. D. An AIEgen/graphene oxide nanocomposite (AIEgen@ GO)‐based two‐stage “turn‐on” nucleic acid biosensor for rapid detection of SARS‐CoV‐2 viral sequence. *Aggregate* **2023**, *4* (1), e195.
(43) Zhang, Q.; Yin, B.; Huang, Y.; Gu, Y.; Yan, J.; Chen, J.; Li, C.; Zhang, Y.; Wong, S. H. D.; Yang, M. A dual “turn-on” biosensor based on AIE effect and FRET for in situ detection of miR-125b biomarker in early Alzheimer's disease. *Biosens. Bioelectron.* **2023**, *230*, 115270.

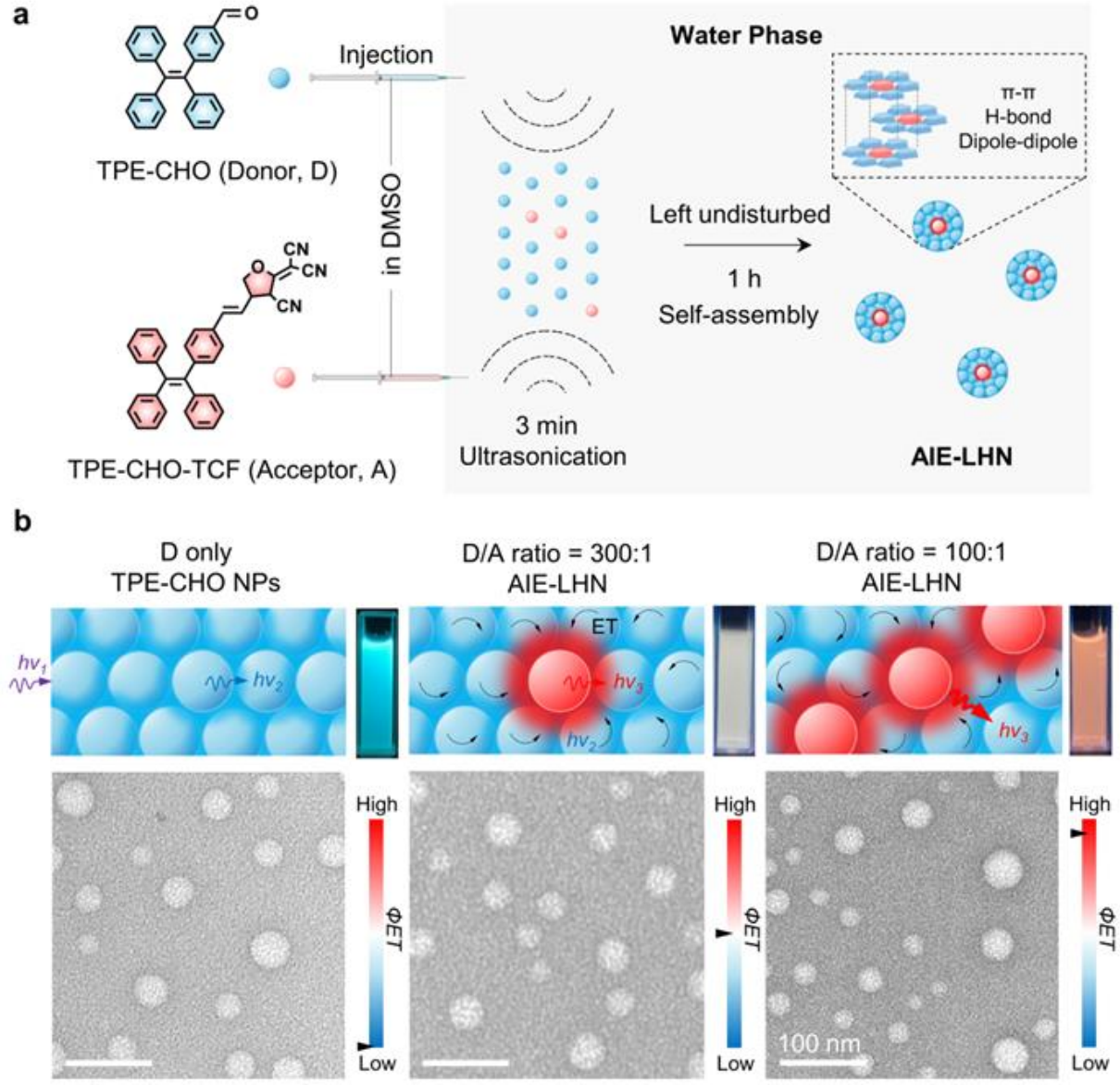


**Figure 1.** One-pot synthesis of scaffold-free AIEgen-based light harvesting nanoparticle (AIE-LHN). (a) The synthesis route of the efficient light harvesting nanosystem based on a pair of AIEgens. (b) Schematic illustration of the energy transfer mechanism in the nanosystem with tunable emissions by varying the donor/acceptor ratio and their transmission electron microscope images. ET denotes "Energy transfer"; $\Phi_{ET}$ denotes "Energy transfer efficiency".

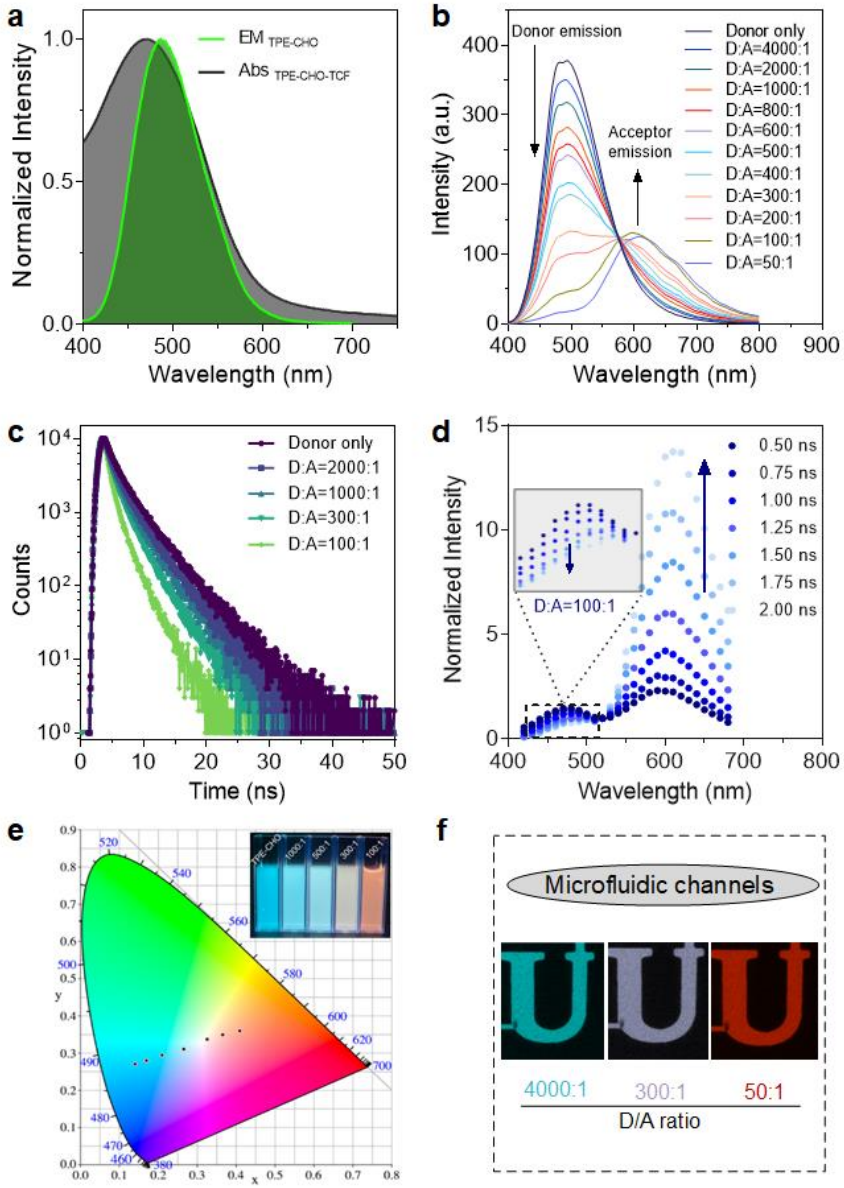


**Figure 2.** Determination of the optical properties of the AIE-LHN. (a) The emission spectrum (EM) of TPE-CHO ($\lambda_{ex}$=372 nm) and absorption spectrum (Abs) of TPE-CHO-TCF. (b) Emission spectra of AIE-LHN with varying D/A ratios ($\lambda_{ex}$=372 nm). (c) Fluorescence decay profiles of AIE-LHN with varying D/A ratios ($\lambda_{ex}$=370 nm and $\lambda_{em}$=485 nm). (d) Time-resolved fluorescence spectra of AIE-LHN at D/A ratio 100:1 after the excitation at 372 nm. (e) CIE 1931 chromaticity diagram showing the luminescence color coordinates of AIE-LHN with varying D/A ratios in water. The inset image shows the corresponding fluorescence photographs under 365 nm UV light. (f) Fluorescence image of the microfluidic channels imprinted with the letter "U" prefilled with AIE-LHN at D/A ratios of 4000:1, 300:1 and 50:1.

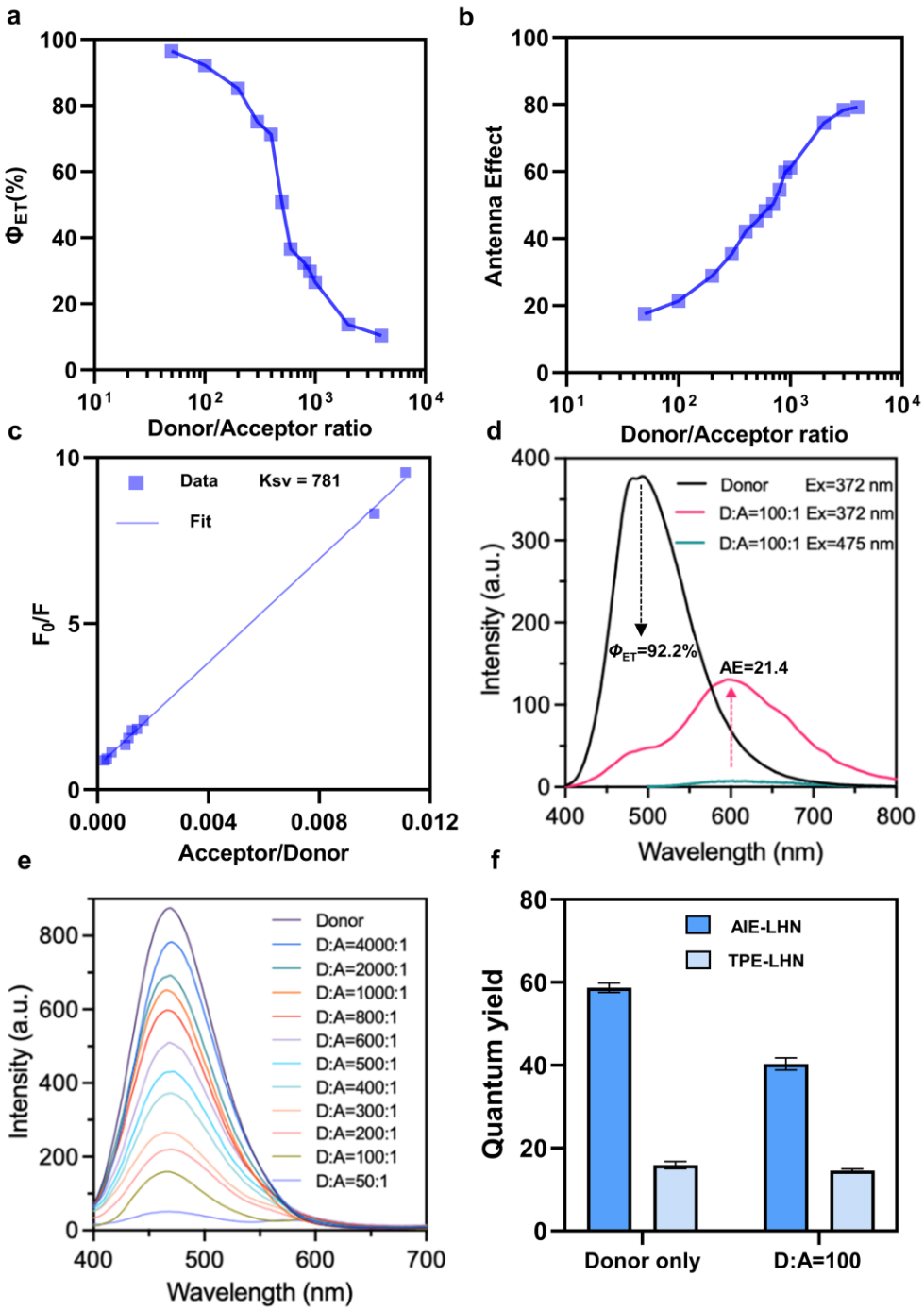


**Figure 3.** Light harvesting performance of AIE-LHN. (a) Energy-transfer efficiencies ($\Phi_{ET}$) and (b) Antenna effect (AE) of AIE-LHN at various D/A ratios. (c) The average number of donor molecules quenched by a single acceptor (Ksv) in AIE-LHN. (d) The emission spectrum of AIE-LHN at the D/A ratio of 100:1. (e) Emission spectra of TPE-LHN at various D/A ratios. (f) Fluorescence quantum yield of AIE-LHN and TPE-LHN with only donor and the donor/acceptor ratio of 100:1, respectively ($\lambda_{ex}$=372 nm).

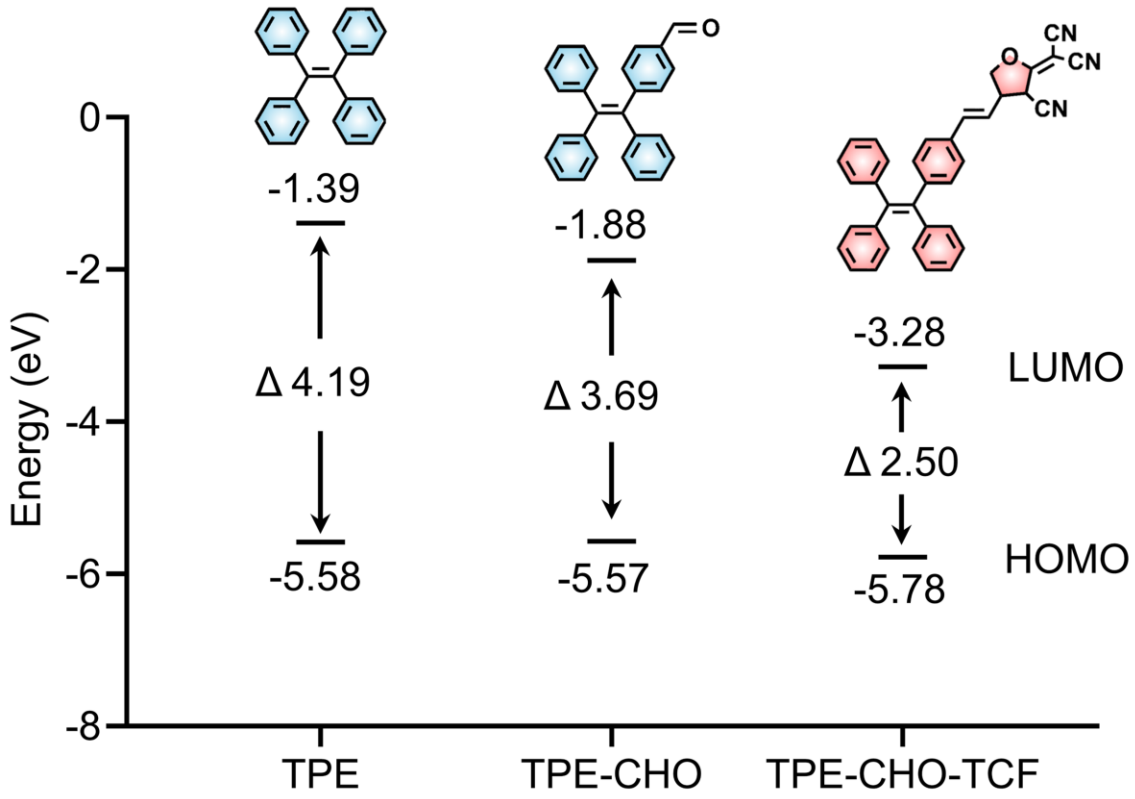


**Figure 4.** Theoretical calculations of the HOMO/LUMO energies for the donors and acceptor.

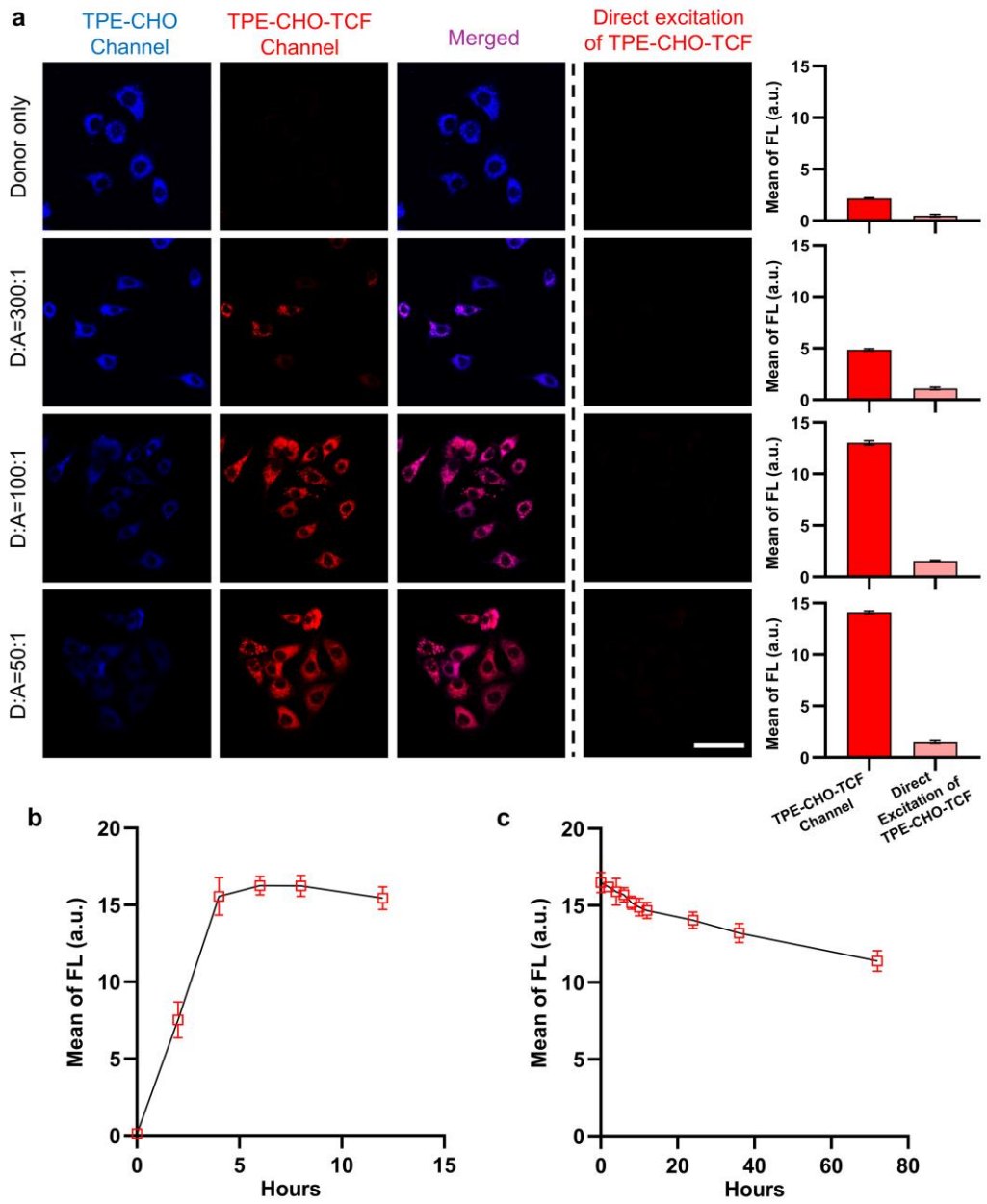


**Figure 5.** Evaluation of the bioimaging performance of AIE-LHN in vitro. (a) Confocal images of the MCF-7 cells after incubation with AIE-LHN of various D/A ratios for 4 h at 37 ºC and 5% $CO_2$ ($\lambda_{ex}$=405 nm, $\lambda_{em}$=650-750 nm channels). The signal emitted from the direct excitation of TPE-CHO-TCF in AIE-LHN ($\lambda_{ex}$=488 nm) was used as a control without energy transfer from donors. Scale bar = 100 μm. (b) The change of cellular TPE-CHO-TCF channel fluorescent intensity during uptaking AIE-LHN (D/A ratio=100:1) over 12 h. (c) Time evolution of the cellular fluorescent intensity of the TPE-CHO-TCF channel in AIE-LHN 4 h post cellular uptake. The incubation concentration of the NPs was 50 μg/mL for all groups.

**Table of Contents**